Structural basis for tropomyosin overlap in thin (actin) filaments and the generation of a molecular swivel by troponin-T

著者	Murakami Kenji, Stewart Murray, Nozawa Kayo, Tomii Kumiko, Kudou Norio, Igarashi Noriyuki, Shirakihara Yasuo, Wakatsuki Soichi, Yasunaga Takuo, Wakabayashi Takeyuki
journal or publication title	Proceedings of the National Academy of Sciences of the United States of America
volume	105
number	20
page range	7200-7205
year	2008-05-20
URL	http://hdl.handle.net/10228/00006522

doi: info:doi/10.1073/pnas.0801950105

Structural basis for tropomyosin overlap in thin (actin) filaments and the generation of a molecular swivel by troponin-T

Kenji Murakami*, Murray Stewart†, Kayo Nozawa*, Kumiko Tomii*, Norio Kudou‡, Noriyuki Igarashi‡, Yasuo Shirakihara§, Soichi Wakatsuki‡, Takuo Yasunaga¶, and Takeyuki Wakabayashi*‖

*Department of Biosciences, School of Science and Engineering, Teikyo University, Toyosatodai 1-1, Utsunomiya 320-8551, Japan; †Laboratory of Molecular Biology, Medical Research Council, Hills Road, Cambridge CB2 0QH, United Kingdom; ‡Structural Biology Research Center, Photon Factory, Institute of Materials Structure Science, High Energy Accelerator Research Organization, Oho 1-1, Tsukuba 305-0801, Japan; §Structural Biology Center, National Institute of Genetics, 1111 Yata, Mishima, Shizuoka 411-8540, Japan; and ¶Department of Bioscience and Bioinformatics, Faculty of Computer Science and Systems Engineering, Kyushu Institute of Technology, Ooaza-kawazu 680-4, Iizuka, Fukuoka 820-850, Japan

Communicated by Chikashi Toyoshima, University of Tokyo, Tokyo, Japan, February 27, 2008 (received for review September 13, 2007)

Head-to-tail polymerization of tropomyosin is crucial for its actin binding, function in actin filament assembly, and the regulation of actin-myosin contraction. Here, we describe the 2.1 Å resolution structure of crystals containing overlapping tropomyosin N and C termini (TM-N and TM-C) and the 2.9 Å resolution structure of crystals containing TM-N and TM-C together with a fragment of troponin-T (TnT). At each junction, the N-terminal helices of TM-N were splayed, with only one of them packing against TM-C. In the C-terminal region of TM-C, a crucial water in the coiled-coil core broke the local 2-fold symmetry and helps generate a kink on one helix. In the presence of a TnT fragment, the asymmetry in TM-C facilitates formation of a 4-helix bundle containing two TM-C chains and one chain each of TM-N and TnT. Mutating the residues that generate the asymmetry in TM-C caused a marked decrease in the affinity of troponin for actin-tropomyosin filaments. The highly conserved region of TnT, in which most cardiomyopathy mutations reside, is crucial for interacting with tropomyosin. The structure of the ternary complex also explains why the skeletal- and cardiac-muscle specific C-terminal region is required to bind TnT and why tropomyosin homodimers bind only a single TnT. On actin filaments, the head-to-tail junction can function as a molecular swivel to accommodate irregularities in the coiled-coil path between successive tropomyosins enabling each to interact equivalently with the actin helix.

calcium | cardiomyopathy | troponin

Tropomyosin, the archetypal coiled-coil protein, is distributed widely in eukaryotic cells where it is a key component of the actin cytoskeleton (1). Tropomyosin molecules lie in the groove of the actin helix and successive molecules overlap head-to-tail so that the C terminus of one binds the N terminus of the next. This overlap is crucial for function, because only polymerizable tropomyosin binds to the actin cytoskeleton, stabilizes its structure, and influences the function of actin-binding proteins, such as ADF/cofilin, Arp2/3, and gelsolin (2, 3). Tropomyosin plays a pivotal role in regulating the actin-myosin interaction in skeletal and cardiac muscle contraction, where its azimuthal position on actin filaments is critical. Cardiac tropomyosin is identical to skeletal α-tropomyosin. At a high Ca^{2+} concentration, tropomyosin equilibrates between two azimuthal positions ("closed" and "open" states). Binding myosin shifts tropomyosin from the closed state (where myosin binds actin only weakly) to the open state (where myosin binds actin strongly) (4, 5). At low Ca^{2+} concentration, the azimuthal shift toward the outer domain of actin is induced by troponin (6, 7) (the "blocked" state, where myosin cannot bind actin).

Sequences of coiled-coil proteins such as tropomyosin contain seven-residue heptad repeats [designated a, b, c, d, e, f, g (8)]. At the interface between the two α-helices, side chains of residues in positions a and d (which are generally hydrophobic) protrude from one helix into the holes between residues on the other helix ["knobs-in-holes" packing (9)]. Some tropomyosin heptad repeats deviate from the canonical pattern in having either bulky or small hydrophobic residues in positions a and d (10). It has been proposed (11) that the small side chains might be able to move within the large holes facilitating the flexibility required for tropomyosin's wide range of functions on actin filaments and this has been verified experimentally (12). Tropomyosin (284 residues in most isoforms) also has a 7-fold (≈40 residue) sequence repeat (13), and each motif is thought to interact similarly with one actin monomer (8, 11).

To accommodate its wide range of functions, tropomyosin exists in >40 isoforms, which are expressed from four genes (1). Each tropomyosin gene is composed of nine exons. Exons 1, 2, 6, and 9 are alternatively spliced, and splicing patterns are correlated with different functions (14). In striated muscle, anchoring the tropomyosin-binding subunit of troponin, troponin-T (TnT, 15), requires the C-terminal region encoded by striated muscle-specific exon 9a (16).

Here, we describe crystal structures of overlapping fragments from the N- and C-terminal regions of tropomyosin in the presence and absence of a fragment of TnT. These structures show how TnT generates a molecular swivel that enables successive tropomyosins to interact equivalently with the actin helix.

Results

Tropomyosin Head–Tail Interaction. The C-terminal (TM-C) (residues 254–284, preceded by a 20 residue fragment of the GCN4 leucine zipper to stabilize dimerization) and N-terminal (TM-N) [residues 1–24, followed by a 12 residue fragment of the GCN4 leucine zipper, and preceded by N-terminal GlyAlaAlaSer-extension necessary to mimic N-acetylation; see refs. 17 and 18 and the top line of supporting information (SI) Fig. S1] regions of skeletal-muscle α-tropomyosin, which is identical to cardiac tropomyosin, were expressed in bacteria (Fig. 1*A*). The structure of $P2_1$ crystals containing both TM-N and TM-C was determined to 2.1 Å resolution by molecular replacement using the C-terminal region of tropomyosin (19) as template. The resultant composite omit map showed that residues 254–281 formed a coiled coil, even though the

Author contributions: K.M. and T.W. designed research; K.M., K.N., K.T., N.K., N.I., Y.S., S.W., T.Y., and T.W. performed research; K.M., M.S., and T.W. analyzed data; and K.M. and T.W. wrote the paper.

The authors declare no conflict of interest.

Data deposition: Coordinates and diffraction data have been deposited in the Protein Data Bank, www.pdb.org [PDB ID codes 2Z5I (binary complex) and 2Z5H (ternary complex)].

‖To whom correspondence should be addressed. E-mail: wakabayashi@nasu.bio.teikyo-u.ac.jp.

This article contains supporting information online at www.pnas.org/cgi/content/full/0801950105/DCSupplemental.

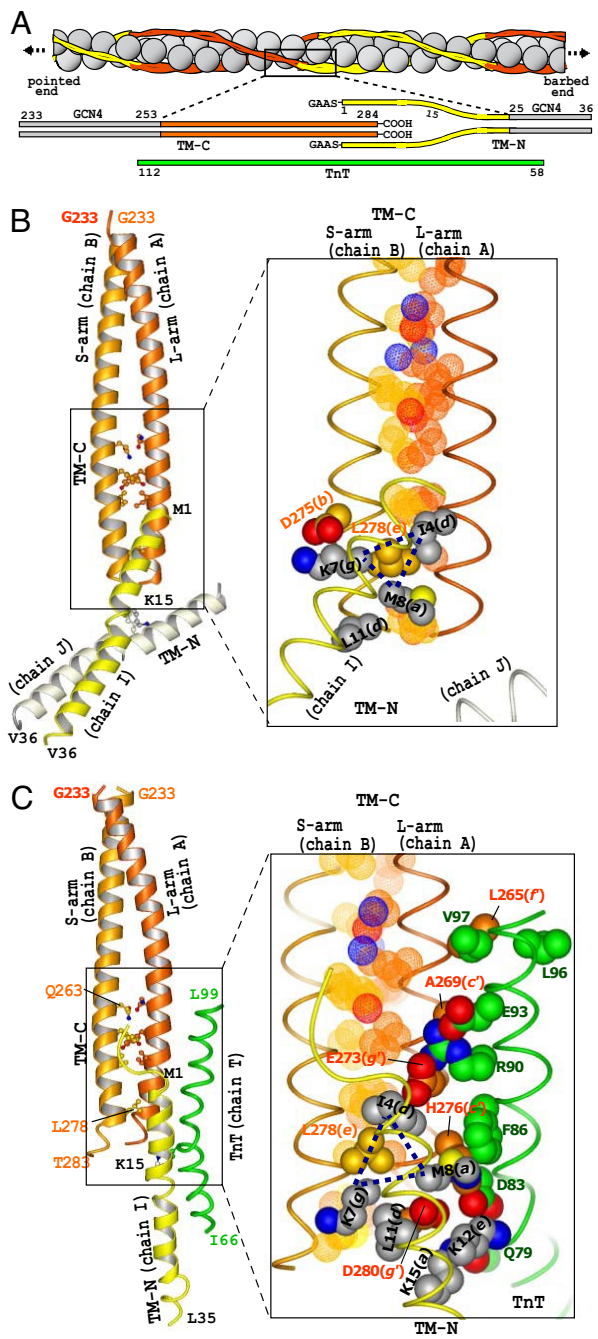

Fig. 1. Overview of the crystal structure of the TM-N:TM-C junction. (*A*) Schematic representation of the constructs used. (*B*) Crystal structure of the binary complex with key residues in ball-and-stick format. The boxed region is enlarged with key residues in CPK format. Leu-278 of TM-C chain B inserts as a knob into a hydrophobic hole (dotted triangle) formed by Ile-4, Lys-7, and Met-8 of TM-N. For simplicity, chains E and F, which bound chain J, are omitted. (*C*) Crystal structure of the ternary complex, with the same TM-C orientation as in *B*. The orientation of the TM-N relative to TM-C differed by ≈50° in comparison with the binary complex.

corresponding region in the template splayed after residue 270 (Fig. S2). After rebuilding TM-C, the difference map showed density for residues 22–36 of both chains of TM-N. After refinement, the model for TM-N could be extended to Met-1 (Fig. 1*B*).

The resultant structure had an R factor of 0.217 (R_{free} = 0.246) and excellent geometry (Table 1). The asymmetric unit contained four TM-C molecules (eight chains: AB, CD, EF, and GH). Although the four TM-C molecules were similar (Cα RMSD = 0.75 Å), the two chains within each molecule were systematically different (Cα RMSD = 0.98 Å). The asymmetric unit contained a single TM-N molecule (two chains: IJ). The TM-N helices were splayed apart from Met-1 to Lys-15 (Fig. 1*B*), of which residues 1–11 interacted with one TM-C. Chains ABCD of TM-C were related to chains EFGH by a noncrystallographic 2-fold axis, which also related chains I and J of TM-N (Fig. 1*B*). Thus, one TM-N molecule interacted with two TM-C molecules and the interaction between chain I and molecule AB was essentially same as that between chain J and molecule EF. The two other TM-C molecules (chains CD and GH) did not interact with a TM-N.

At the TM-N:TM-C junction, hydrophobic residues of TM-N (Met-1 and Met-8 in position *a*; Ile-4 and Leu-11 in position *d*) packed against TM-C, but not against the other TM-N chain (Fig. 1*B*). The TM-N:TM-C interaction showed "knob-in-hole" packing: Leu-278 (position *e*) of the TM-C B chain was inserted as a single knob into a single hydrophobic hole formed by Ile-4, Lys-7, and Met-8 of TM-N (Fig. 1 *B* and *C*). The importance of Leu-278 is highlighted by its conservation (Leu or Phe) between isoforms (Fig. S1) and suggests that in all isoforms except Tmbr2, tropomyosin molecules overlap in a similar way.

A Water Molecule in the Coiled-Coil Core Breaks the Symmetry in the C-Terminal Region of Tropomyosin. Although each TM-C molecule formed a coiled coil over its entire length, the local 2-fold symmetry was broken. One arm [designated L (long)] was more bent and followed a longer path than the other [designated S (short)] (Fig. 2*C*; also see Fig. S3). The asymmetric kink in TM-C appeared to be intrinsic and not induced by TM-N, because the two TM-C molecules (chains CD and GH) in the asymmetric unit that did not associate with TM-N showed similar asymmetric kinks. Tyr-267 and Ile-270 (in positions *a* and *d*, respectively) appeared to be too bulky to fit within the hydrophobic core of a two-stranded canonical coiled coil (Fig. S2*D*). The S-arm (chains BDFH) was more parallel to the L-arm (chains ACEG) in this region (residues 263–270) than in the other part of TM-C, with a smaller crossing angle (Figs. S2*D* and S3), avoiding a steric clash at the interhelical interface. This, in turn, induced the kink of the L-arm near Ile-270 in a plane perpendicular to the broad face, so that two helices formed knobs-in-holes packing after Ile-270 (Fig. S2*D*). Thus, the two broad faces of TM-C were differentiated into convex and concave sides in the C-terminal region of TM-C (Fig. S3*D*). The asymmetry was augmented by a H-bond network and a cation-π interaction on the concave side that included Glu-259, Gln-263, Lys-264, Lys-266, and Tyr-267 (Fig. 2*C*). The H-bond network was stabilized by two waters, one of which was in the coiled-coil core. This unusual water was located slightly nearer to the L-arm (Fig. 2 *A* and *B*) and participated in the H-bond network only on the concave side. A H-bond network was not observed on the convex side, where the corresponding residues adopted more variable conformations (RMSD 0.84 Å vs. 0.58 Å on the concave side).

The asymmetry introduced by the kink was crucial in the formation of the head-to-tail junction, because the side chain of Met-281 of the L-arm folded back onto L-arm Leu-278, hindering its functioning as a knob (Fig. 2*C* and Fig. S3*D*). On the convex side, S-arm Leu-278 was free to bind TM-N. This may explain why tropomyosin overlaps with only a single molecule rather than two, as would be expected if its chains were related by a strict 2-fold. Notably, residues 263 (Gln or Glu), 266 (Lys or Arg), Tyr-267, and Ile-270, which are responsible for the asymmetric kink, are conserved only in striated-muscle isoforms (Fig. S1), suggesting the asymmetric structure of the C-terminal region of tropomyosin may be striated-muscle specific and is required to anchor TnT. The affinity of TnT for tropomyosin on actin filaments decreased after Y267N and I270L mutations (Fig. S4).

The TM-N coiled coil was disrupted at Lys-15 where the chains

Table 1. Crystallographic statistics

Statistics	TM-C:TM-N binary complex	TM-C:TM-N:TnT ternary complex
Data collection		
Space group	$P2_1$	$I2_12_12_1$
Unit cell dimensions, Å	a = 41.957	a = 84.809
	b = 114.498	b = 158.308
	c = 68.351	c = 163.570
Resolution range, Å	65–2.10 (2.18–2.10)*	113–2.89 (3.00–2.89)*
Wilson B-factor	28.5	70.8
Total observations	81,232	121,225
Unique reflections	35,852	25,479
Completeness, %	96.5 (96.7)*	96.5 (95.5)*
R_{merge}, %	6.5 (29.9)*	7.7 (31.7)*
I/σ	13.6 (3.8)*	9.6 (2.8)*
Refinement		
R_{cryst}/R_{free}, %	21.7/24.6 (65–2.10 Å)	23.6/24.7 (113–2.89 Å)
Total no. of non-H atoms	4,147 (320 water molecules)	3,946 (55 water molecules)
Average B factors of backbone atoms		
233–253 of TM-C, Å^2	22.70	42.24
254–262 of TM-C, Å^2	19.25	41.42
263–270 of TM-C, Å^2	29.93	44.58
271–283 of TM-C, Å^2	72.76	64.10
TM-N, Å^2	78.60	169.68
TnT, Å^2	—	195.60
Ramachandran plot		
Core region, %	98.2	93.6
Allowed region, %	1.8	5.1
Generously allowed region, %	0.0	1.3
Disallowed region, %	0.0	0.0

Dash indicates not applicable.
*Values in parentheses refer to final resolution shell.

splayed apart (Fig. 3*A*). The side chains of Ala-18 (position *d*) and Ala-22 (position *a*) in the coiled-coil core were close to each other, and the interhelix distance (7.2–7.6 Å) was much shorter than that for canonical coiled coils (9–10 Å). This close packing hindered the large side chain of Lys-15 (position *a*) from fitting into the core. These residues are conserved between isoforms (Fig. S1), indicating that the deviation from canonical coiled coil in the N-terminal region is common to all isoforms.

Mutagenesis confirmed that the N-terminal splaying was not a crystal packing artifact and was indeed important for tropomyosin polymerization and actin binding. Three residues (Lys-15, Ala-18, and Ala-22) thought to be major contributors to the splaying were mutated to Leu to facilitate formation of a canonical coiled coil. This triple-L mutant showed almost no actin binding (Fig. 3*B* and Fig. S4), consistent with polymerization being hindered. The importance of N-terminal splaying was further illustrated by cross-linking the N termini of full-length tropomyosin by air-oxidization of introduced cysteines. Actin binding of the M1C mutant was markedly decreased, but rescued by reduction with DTT, whereas cross-linking at the C terminus (using the I284C mutant) was much less disruptive (Fig. 3*B* and Fig. S4).

TM-N:TM-C:TnT Ternary Complex. We obtained $I2_12_12_1$ crystals containing TM-N, TM-C, and chicken skeletal TnT residues 58–112 (Fig. 1*C*) that diffracted to 2.9 Å resolution (Table 1). Molecular replacement found four TM-C's in the asymmetric unit that were all similar to those in the binary complex (Fig. S3*C*). After rebuilding the TM-Cs, the difference map showed additional density, attributable to TM-N (chain I) and TnT (chain T), which bound to one of the four TM-C molecules in the asymmetric unit. Electron density corresponding to the other TM-N chain (the coiled-coil mate of chain I) was not clear, although there was some vague density that might correspond to residues 27–29. The TnT chain (residues 66–99) interacted with both the L-arm of TM-C and the I chain of TM-N in an antiparallel orientation that was consistent with the 17 Å resolution crystal structure of tropomyosin-troponin (16). Interacting residues of TnT generally coincided with the highly conserved region (residues 69–112) in which many cardiomyopathy mutations (such as F86I) are found (20).

Although the angle between their axes differed (Fig. 1 *B* and *C*), the general features of the TM-N:TM-C interaction in the ternary complex were similar to those in the binary complex. Ile-4, Lys-7, and Met-8 of TM-N showed similar "knob-in-hole" packing onto TM-C (Fig. 1*C*). The changed orientation of TM-N relative to TM-C may be related to the small interaction interface at the junction, which buried only 165 Å^2 of surface area in the binary complex, and is consistent with the weak head-to-tail interaction (K_d 10–100 μM).

The TM-C molecules in the ternary complex showed the same symmetry breaking observed in the binary complex (Fig. S3*C*), confirming that this was a general feature of tropomyosin and not due to crystal packing. The kink appeared to be essential for TnT binding, because it allowed close packing between the L-arm and TnT with the optimal helix-crossing angle (21) of ≈18°. Moreover, the kink provided a space for the side chains of the L-arm (His-276 and Asp-280) and those of TnT (Asp-83 and Phe-86) to interact with TM-N (Leu-11, Lys-12, and Lys-15) (Fig. 1*C*). His-276 of the L-arm faced against Phe-86 of TnT. This Phe-86 corresponds to cardiac Phe-110, mutation of which causes hypertrophic cardiomyopathy and weakens the affinity of troponin to actin-tropomyosin (20). Were the L-arm less kinked, the C-terminal region would clash with the TM-N and TnT chains. The asymmetry introduced by kink in TM-C explains why homodimeric tropomyosin binds only a single troponin even in the absence of actin (22).

Four-Helix Bundle Formation in the Ternary Complex. Where they overlapped, the two TM-C chains, TM-N chain, and TnT chain

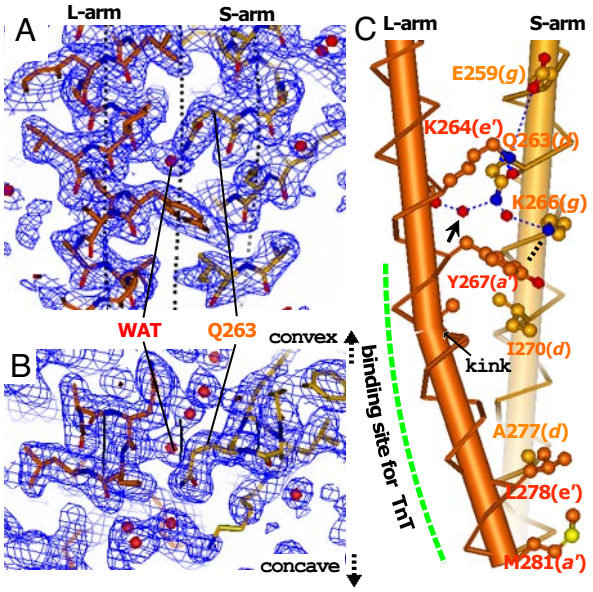

Fig. 2. Asymmetric architecture of the TM-C coiled coil. (*A*) Side views of the coiled coil showing the key water molecule in its hydrophobic core in the 2Fo-Fc composite omit map (contoured at 1σ) of the binary complex. This water interacts differently with each TM-C chain and breaks the local 2-fold symmetry. Faint lines show the α-helical and coiled-coil axes traced with TWISTER (35). (*B*) Oblique view rotated around the horizontal axis by 60° with respect to *A*. Stereoview is shown in Fig. S9*D*. (*C*) Kink of the L-arm near Tyr-267 differentiates the convex and concave coiled-coil faces with the key residues shown in ball-and-stick format. Arrow indicates the key water in the coiled-coil core. Dotted blue lines indicate putative H-bonds.

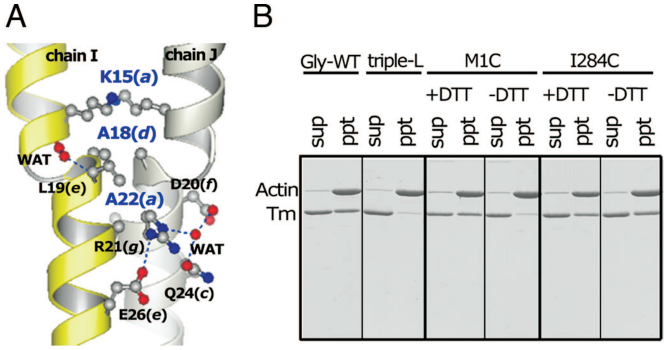

Fig. 3. Disruption of the coiled coil in the N-terminal region of tropomyosin. (*A*) Disruption of the coiled coil in residues 15–22 of TM-N in the binary complex. Dotted lines indicate putative salt bridges or H-bonds. The side chains of Ala-18 and Ala-22 and those of their coiled-coil mates were close to each other. The close interhelix packing was reinforced by salt bridges and H-bonds (dotted lines), including Asp-20, Arg-21, Gln-24, and Glu-26. (*B*) Binding assay showing that splaying of the N-terminal region of tropomyosin is necessary for stable binding to actin filaments. Tropomyosin mutants (1.95 μM) were cosedimented with actin (2.3 μM).

formed an asymmetric four-helix bundle >18 Å long (Fig. 4). Although the electron density due to the I and T chains was weaker than that for the TM-C molecules, the backbone of the TM-N and TnT chains could be traced clearly in composite omit maps (Fig. S5, Fig. S6, and Fig. S7). The four additional N-terminal residues of TM-N extended along the S-arm of TM-C (Fig. 4 *A* and *C*), consistent with the extension in nonmuscle isoforms strengthening binding at the junction (18). TnT packed more tightly against the L-arm of TM-C (buried surface area 469 Å^2) than against TM-N (buried surface area 224 Å^2). The interhelix distance from TnT to the L-arm of TM-C (≈9 Å) was shorter than that to the I chain of TM-N (≈15 Å) (Fig. 4*B*). The helix axis of TnT was bent by 15° between Ala-80 and Asp-83 (Fig. 4*A*), where the backbone H-bonds were disrupted and instead intermolecular H-bonds appeared to be formed between the carbonyls of Asp-83 and Ala-80 of TnT and the side chains of His-276 of TM-C (L-arm) and Lys-12 of TM-N, respectively (Fig. 4*A*). The difference in the extent and tightness of the interhelix interactions can explain, in part, why striated-muscle specific C-terminal exon9 (residues 258–284) is

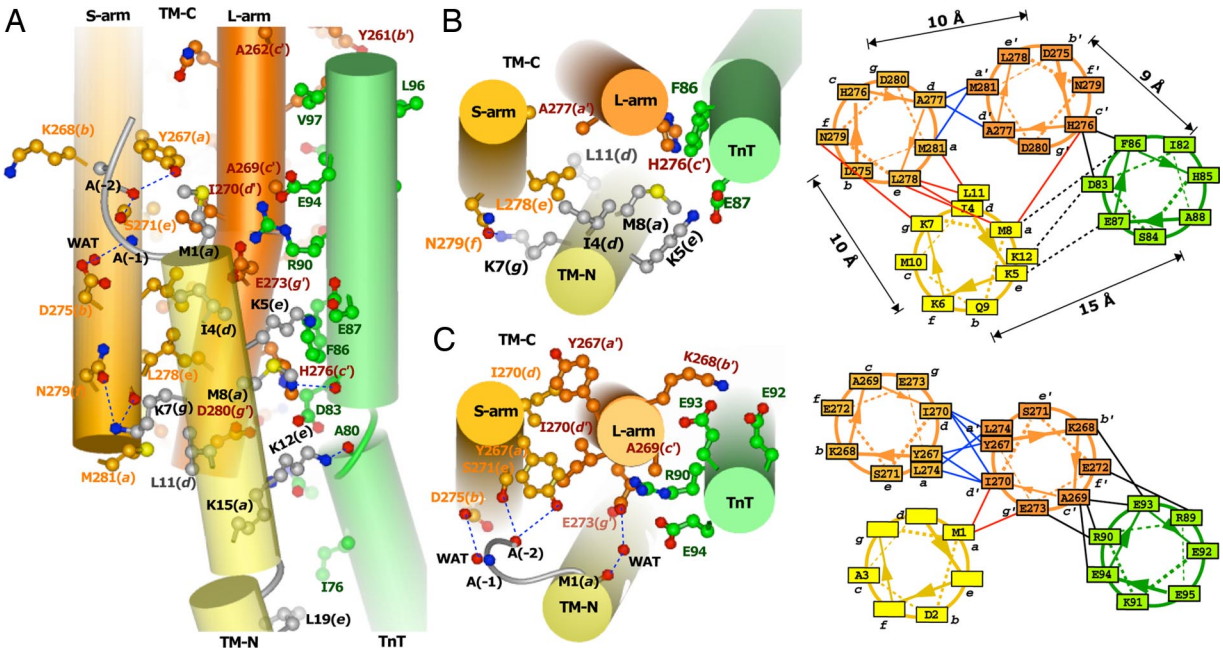

Fig. 4. Intermolecular interfaces around the junctional region in the ternary complex. (*A*) The four-helix bundle structure in the TM-N:TM-C:TnT complex viewed from the convex side. Dotted lines indicate putative H-bonds. (*B* and *C*) Views of the junctional region in the ternary complex at two different levels together with schematic illustrations (*Right*) showing interacting residues. Solid blue lines represent the intramolecular interactions between the S- and L-arms of TM-C.

more important for binding TnT than the N-terminal exon1 (residues 1–38) (14, 23). The tight packing of TnT with the L-arm with small residues in every seventh position was similar to that in "Alacoil" (21), which is a common motif in tightly packed antiparallel coiled coils that allows close interhelix spacing (≈7.5–8.5 Å). Ala-269 (c') and probably Ala-262 (c') of the L-arm appeared to play a similar role for its tight packing to TnT (Fig. 4*A*). The methyl group of Ala-269 of the L-arm was surrounded by the hydrophobic aliphatic chains of Arg-90, Glu-93, and Glu-94 of TnT (Fig. 4*C*). The average *B* factor (≈170 Å^2) of residues 85–95 of TnT was lower than other regions of TnT, and R_{free} decreased significantly when residues 85–95 were incorporated to the model.

Discussion

The structure of the overlap between TM-N and TM-C in both the binary and ternary complexes was asymmetric, with the N termini of TM-N being splayed. This arrangement differed from that in an NMR structure (24) of the junction, which is symmetric with splayed C termini. The crystal structures of C-terminal fragments in the absence of the N-terminal fragment showed a tail-tail interaction with splayed C termini (19, 25). These results indicate that the C-terminal region can take up multiple configurations including a splayed one. However, the results we obtained with full-length tropomyosin mutants (Fig. 3*B*) suggested that, whereas splaying of the N termini is required for stable actin binding, splaying at the C termini is not. The symmetric NMR structure might have been produced because the TM-N fragment used terminated at Asp-14. Our longer TM-N fragment retained residues 1–24 and crucially contained Lys-15, Ala-18, and Ala-22, which are important to form the junction with the splayed N termini (Fig. 3*A*).

Implications for Regulation of Striated Muscle Contraction. A crucial feature of the disruption of the tropomyosin coiled coil in the junction is that it enables successive molecules to interact with actin in an equivalent manner. The local disruption of the coiled coil acts as a molecular swivel that allows successive molecules to rotate relative to one another around the axis of coiled coil. In their original analysis of the actin-tropomyosin interaction, Stewart and McLachlan (8) proposed that the coiled-coil path would have to be maintained between successive tropomyosin molecules to enable each to interact with seven actins in an approximately equivalent manner (Fig. 5*A*). To achieve this, they proposed that the tropomyosin coiled-coil pitch was 137 Å and that successive molecules overlapped by 7–11 residues in a way that did not result in an abrupt change in coiled-coil rotation. Subsequent work indicated that, at least in some instances, the rotation angle of the coiled coil changes by ≈90° between successive molecules (24, 26). Such a change would mean that the interaction geometry between alternate tropomyosins and actin would be different. The swivel action at the junction is crucial for resolving this dilemma. By splaying the N terminus and binding to only one chain, TnT helps disrupt the coiled coil locally, enabling it to accommodate the change in the rotation angle between successive tropomyosins along an actin filament.

Rotation Angle of Tropomyosin Around Its Axis. Although the torsional rigidity of a coiled coil is probably not high, it would still be difficult for an intact coiled coil to have strictly equivalent interactions with each of seven actin monomers. Analysis of EM reconstructions of thin filaments support a pseudoequivalent interaction (6). At both high and low Ca^{2+} concentrations, the rotation angle of tropomyosin in the N-terminal half (blocks I–IV) is different from that in the C-terminal half (blocks V–VII) (Fig. 5), so that the coiled coil is untwisted relative to the strictly equivalent binding model illustrated in Fig. 5*A*. The way TM-N, TM-C, and TnT interact would enable the discontinuity of the coiled-coil path between successive tropomyosins to be accommodated. The residual difference in rotation angle may differentiate the actin-tropomyosin interactions and cause the different behavior of the N-terminal and C-terminal halves of tropomyosin, in which blocks V–VII appear to change its azimuthal position on actin filaments more dramatically than blocks II–IV upon Ca^{2+}-regulation (6).

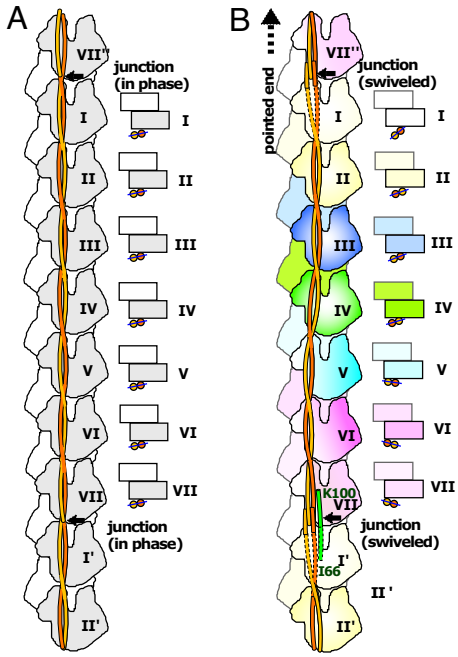

Fig. 5. Proposed models of actin-tropomyosin filaments. For simplicity, the actin double helix is untwisted. (*A*) The strictly equivalent binding model of actin-tropomyosin filaments deduced from tropomyosin sequence analysis (8). The coiled-coil path is maintained between successive tropomyosins to enable each to interact with seven actins in an approximately equivalent manner. Schematic top views of cross-sections at the level of actin Pro-333 are shown at *Right*. Views are from the actin filament pointed end. Two contacting circles and rectangles represent helices of the coiled coil of tropomyosin and double helix of actin, respectively. (*B*) Model of a filament containing actin, tropomyosin, and troponin T deduced from analysis of the cryo-EM map of thin filament (actin-tropomyosin-troponin at high Ca^{2+} concentration) (6). The coiled coil was slightly untwisted relative to the strictly equivalent binding model in *A*. Thin filament containing both troponin and tropomyosin is divided into seven axial blocks (designated I through VII) corresponding to individual actin chains. The model shows how the swivel can accommodate a change in coiled-coil rotation angle at the junction.

The crystal structure of the ternary complex provided a key to determine the rotation angle of tropomyosin around its axis in block VII at high Ca^{2+} concentration more precisely, because the ternary complex could be docked into the EM map only when its concave side was put against actin (Fig. 5*B*). On this side, more hydrophobic residues of TM-C and TnT were exposed, whereas more polar residues were exposed on the other side. Consistent with this interpretation, the ternary complex bound to actin filaments more strongly with addition of salt (Fig. S8). Importantly, it is likely that TnT helped generate a shift of the azimuthal position of tropomyosin in blocks V–VII toward the inner domain by ≈7 Å relative to that in blocks II–IV at high Ca^{2+} concentration (Fig. 5*B*). These two azimuthal positions probably correspond to the closed state, where myosin binds actin weakly, and the open state, where myosin binds actin strongly. This is because, in each of blocks II–IV, tropomyosin blocked actin Pro-333, which has been suggested to be included in the strong-binding site for myosin (4, 27), whereas the Pro-333 in blocks V and VI was free to bind myosin. In block VII, Pro-333 of actin was occupied by TnT and myosin cannot bind strongly. Biochemical data also has suggested that TnT modulates the equilibrium between closed and open states (28). The proposed

azimuthal shift of tropomyosin between blocks IV and V is supported by tropomyosin crystal structures (29), which showed that the coiled coil is disturbed around residues 151–162, located in the C-terminal half of block IV. The flexibility generated by an alanine cluster (Ala-151, 155, and 158) and nearby Tyr-162 in the coiled-coil core would also help accommodate the difference in the azimuthal position between blocks IV and V. When the alanine cluster (156–162) is replaced, the actin-activated myosin ATPase is suppressed (30). In block I, the EM density corresponding to tropomyosin was too weak to determine the azimuthal position of tropomyosin unambiguously (6). However, the joint-rotation of TM-N at the junction (Fig. 1 *B* and *C*) and the discontinuity of the TnT helix at the residues 80–83 (Fig. 4*A*) might also accommodate the stress produced by the azimuthal shift of tropomyosin between successive molecules (Fig. 5*B*).

The molecular swivel generated by TnT at the junction between successive tropomyosins is thus crucial to facilitate a range of interactions with actin that are fundamental to the regulation of striated muscle contraction.

Materials and Methods

Protein Expression, Purification, and Crystallization. Rabbit striated-muscle α-tropomyosin TM-C (residues 254–284, preceded by a 20-residue fragment of the GCN4 leucine zipper), TM-N [residues 1–24, followed by a 12-residue fragment of the GCN4 leucine zipper, and preceded by an N-terminal extension (AAS)], and chicken skeletal TnT (residues 58–112) were expressed in *Escherichia coli*. Vapor diffusion was used to generate crystals of the binary and ternary complex, using well buffers containing 100 mM Mes (pH6.5), 10 mM Tris·HCl (pH7.5), 150 mM NaCl, 50 mM $Mg(OAc)_2$, 100 mM $CaCl_2$ and 10% PEG3350, and 100 mM Na-cacodylate (pH 6.5), 10 mM Tris·HCl, 150 mM NaCl, 250 mM $MgCl_2$ and 10% PEG 8000, respectively.

Structure Determination and Refinement. Details are described in *SI Materials and Methods*. In brief, the structure of the ternary complex was solved by molecular replacement (31), using the C-terminal region of tropomyosin (19) as an initial model. After rebuilding and refinement of TM-C, using O (ref.32) and CNS (ref.33), a composite omit map showed interpretable α-helical densities for TM-N and TnT. The model was refined with Refmac5 (34). Structure of the binary complex was solved by molecular replacement in the similar manner. Coordinates and structure factors for the binary and ternary complexes have been deposited in the Protein Data Bank (www.pdb.org), with ID codes 2Z5I and 2Z5H, respectively.

Binding Assays. Each tropomyosin mutant (1.95 μM) was mixed with 2.3 μM actin in 63 mM NaCl, 20 mM imidazole·HCl (pH 7.0), 3 mM $MgCl_2$, 100 μM $CaCl_2$, 1 mM ATP, and 2.3 μM phalloidin with or without 50 mM DTT. The mixture was incubated for 30 min at 25°C, centrifuged, and analyzed by SDS/PAGE.

ACKNOWLEDGMENTS. We thank Dr. M. Kawamoto of SPring-8 and the staff of the Photon Factory (proposal nos. 2005G292 and 2006G375) for assistance with data collection; Prof. T. Tsukihara for allowing us to collect data with BL44XU at SPring-8; Drs. Y. Matsuura, O. Nureki, and A. Houdusse for advice on molecular replacement; Drs. Y. Maeda (Nagoya University, Japan) and K. Maeda (Nagoya University, Japan) for the gift of tropomyosin cDNA; Dr. F. Reinach (University of São Paulo, Brazil) for sending troponin cDNA; and Drs. K. Sutoh, T. Uyeda, T. Noguchi, and Y. Amano for molecular biology assistance. This work was supported by the Human Frontier Science Program and a Grant-in-Aid for Scientific Research on Priority Areas from the Ministry of Education, Science, Technology and Sports of Japan (to T.W.).

1. Lees-Miller JP, Helfman DM (1991) The molecular basis for tropomyosin isoform diversity. *Bioessays* 13:429–437.
2. Pollard TD, Borisy GG (2003) Cellular motility driven by assembly and disassembly of actin filaments. *Cell* 112:453–465.
3. Gunning PW, Schevzov G, Kee AJ, Hardeman EC (2005) Tropomyosin isoforms: Divining rods for actin cytoskeleton function. *Trends Cell Biol* 15:333–341.
4. Toyoshima C, Wakabayashi T (1985) Three-dimensional image analysis of the complex of thin filaments and myosin molecules from skeletal muscle. V. Assignment of actin in the actin-tropomyosin subfragment-1 complex. *J Biochem* 97:245–263.
5. McKillop DE, Geeves MA (1993) Regulation of the interaction between actin and myosin subfragment 1: Evidence for three states of the thin filament. *Biophys J* 65:693–701.
6. Narita A, Yasunaga T, Ishikawa T, Mayanagi K, Wakabayashi T (2001) Ca^{2+}-induced switching of troponin and tropomyosin on actin filaments as revealed by electron cryo-microscopy. *J Mol Biol* 308:241–261.
7. Murakami K, *et al.* (2005) Structural basis for Ca^{2+}-regulated muscle relaxation at interaction sites of troponin with actin and tropomyosin. *J Mol Biol* 352:178–201.
8. Stewart M, McLachlan AD (1975) 14 actin binding sites on tropomyosin? *Nature* 257:331–333.
9. Crick FHC (1957) The packing of α-helices: Simple coiled-coils. *Acta Crystallogr* 6:689–697.
10. Stewart M (2001) Structural basis for bending tropomyosin around actin in muscle thin filaments. *Proc Natl Acad Sci USA* 98:8165–8166.
11. McLachlan AD, Stewart M (1976) The 14-fold periodicity in α-tropomyosin and interaction with actin. *J Mol Biol* 103:271–298.
12. Brown JH, *et al* (2001) Structure of the mid-region of tropomyosin: Bending and binding sites for actin. *Proc Natl Acad Sci USA* 98:8496–8501.
13. McLachlan AD, Stewart M (1975) Tropomyosin coiled-coil interactions. *J Mol Biol* 98:293–304.
14. Moraczewska J, Nicholson-Flynn K, Hitchcock-DeGregori SE (1999) The ends of tropomyosin are major determinants of actin affinity and myosin subfragment 1-induced binding to F-actin in the open state. *Biochemistry* 38:15885–15892.
15. Ebashi S, Wakabayashi T, Ebashi F (1971) Troponin and its components. *J Biochem* 69:441–445.
16. White SP, Cohen C, Phillips GN, Jr (1987) Structure of co-crystals of tropomyosin and troponin. *Nature* 325:826–828.
17. Hitchcock-DeGregori SE, Heald RW (1987) Altered actin and troponin binding of amino-terminal variants of chicken striated muscle alpha-tropomyosin expressed in *Escherichia coli*. *J Biol Chem* 262:9730–9735.
18. Monteiro PB, Lataro RC, Ferro JA, Reinach FC (1994) Functional alpha-tropomyosin produced in Escherichia coli. A dipeptide extension can substitute the amino-terminal acetyl group. *J Biol Chem* 269:10461–10466.
19. Li Y, *et al.* (2002) The crystal structure of the C-terminal fragment of striated-muscle alpha-tropomyosin reveals a key troponin T recognition site. *Proc Natl Acad Sci USA* 99:7378–7383.
20. Hinkle A, Tobacman LS (2003) Folding and function of the troponin tail domain. Effects of cardiomyopathic troponin T mutations. *J Biol Chem* 278:506–513.
21. Gernert KM, Surles MC, Labean TH, Richardson JS, Richardson DC (1995) The Alacoil: A very tight, antiparallel coiled-coil of helices. *Protein Sci* 4:2252–2260.
22. Pato MD, Mak AS, Smillie LB (1981) Fragments of rabbit striated muscle alpha-tropomyosin. I. Preparation and characterization. *J Biol Chem* 256:593–601.
23. Hammell RL, Hitchcock-DeGregori SE (1996) Mapping the functional domains within the carboxyl terminus of alpha-tropomyosin encoded by the alternatively spliced ninth exon. *J Biol Chem* 271:4236–4242.
24. Greenfield NJ, *et al.* (2006) Solution NMR structure of the junction between tropomyosin molecules: Implications for actin binding and regulation. *J Mol Biol* 364:80–96.
25. Nitanai Y, Minakata S, Maeda K, Oda N, Maeda Y (2007) Crystal structures of tropomyosin: Flexible coiled-coil. *Adv Exp Med Biol* 592:137–151.
26. Whitby FG, Phillips GN, Jr (2000) Crystal structure of tropomyosin at 7 Angstroms resolution. *Proteins* 38:49–59.
27. Milligan RA (1996) Protein–protein interactions in the rigor actomyosin complex. *Proc Natl Acad Sci USA* 93:21–26.
28. Maytum R, Geeves MA, Lehrer SS (2002) A modulatory role for the troponin T tail domain in thin filament regulation. *J Biol Chem* 277:29774–29780.
29. Brown JH, *et al.* (2005) Structure of the mid-region of tropomyosin: Bending and binding sites for actin. *Proc Natl Acad Sci USA* 102:18878–18883.
30. Sakuma A, *et al.* (2006) The second half of the fourth period of tropomyosin is a key region for Ca^{2+}-dependent regulation of striated muscle thin filaments. *Biochemistry* 45:9550–9558.
31. Storoni LC, McCoy AJ, Read RJ (2004) Likelihood enhanced fast rotation functions. *Acta Crystallogr D* 60:432–438.
32. Jones TA, Zou JY, Cowan SW, Kjeldgaard M (1991) Improved methods for building protein models in electron density maps and for locating errors in these models. *Acta Crystallogr A* 47:110–119.
33. Brunger AT, *et al.* (1998) Crystallography & NMR system: A new software suite for macromolecular structure determination. *Acta Crystallogr D* 54:905–921.
34. Collaborative Computational Project, Number 4 (1994) The CCP4 suite: Programs for protein crystallography. *Acta Crystallogr D* 50:760–763.
35. Strelkov SV, Burkhard P (2002) Analysis of α-helical coiled coils with the program TWISTER reveals a structural mechanism for stutter compensation. *J Struct Biol* 137:54–64.